Nanonet force microscopy for measuring forces in single smooth muscle cells of the human aorta

Alexander Hall[a], Patrick Chan[b], Kevin Sheets[c], Matthew Apperson[a], Christopher Delaughter[a], Thomas G. Gleason[b,d], Julie A. Phillippi[b,d,*], and Amrinder Nain[a,c,*]

[a]Department of Mechanical Engineering and [c]Department of Biomedical Engineering and Sciences, Virginia Tech, Blacksburg, VA 24061; [b]Department of Cardiothoracic Surgery and [d]Department of Bioengineering and McGowan Institute for Regenerative Medicine, University of Pittsburgh, Pittsburgh, PA 15219

ABSTRACT **A number of innovative methods exist to measure cell–matrix adhesive forces, but they have yet to accurately describe and quantify the intricate interplay of a cell and its fibrous extracellular matrix (ECM). In cardiovascular pathologies, such as aortic aneurysm, new knowledge on the involvement of cell–matrix forces could lead to elucidation of disease mechanisms. To better understand this dynamics, we measured primary human aortic single smooth muscle cell (SMC) forces using nanonet force microscopy in both inside-out (I-O intrinsic contractility) and outside-in (O-I external perturbation) modes. For SMC populations, we measured the I-O and O-I forces to be 12.9 ± 1.0 and 57.9 ± 2.5 nN, respectively. Exposure of cells to oxidative stress conditions caused a force decrease of 57 and 48% in I-O and O-I modes, respectively, and an increase in migration rate by 2.5-fold. Finally, in O-I mode, we cyclically perturbed cells at constant strain of varying duration to simulate in vivo conditions of the cardiac cycle and found that I-O forces decrease with increasing duration and O-I forces decreased by half at shorter cycle times. Thus our findings highlight the need to study forces exerted and felt by cells simultaneously to comprehensively understand force modulation in cardiovascular disease.**

Monitoring Editor
Diane Lidke
University of New Mexico

Received: Jan 23, 2017
Revised: Apr 6, 2017
Accepted: Apr 18, 2017

INTRODUCTION

Smooth muscle cells (SMCs) receive mechanical and chemical stimuli from the extracellular matrix (ECM) via integrin-mediated focal adhesions (Moiseeva, 2001). For a vascular SMC, this interaction plays an important role in modulating vascular resistance and tone, thereby affecting the resistance of a vessel. SMCs generate forces via actomyosin contractions, which impart a mechanical force on the surrounding ECM (Gunst and Zhang, 2008). This leads to vasoconstriction or dilatation of vessels, affecting overall systemic vascular resistance. Furthermore, in the arterial system, particularly in the aorta, there is an ECM-directed force generated by contraction in the cardiac cycle, which is experienced by the SMCs. The pulsatility causes the collagen and elastin microarchitecture to stretch, and the resulting stretch force is transmitted through the focal adhesions to the cytoskeletal network.

Establishing a contextually relevant fibrous platform to understand cell-generated (inside-out [I-O]) and ECM-generated (outside-in [O-I]) forces is integral to the study of disease states. At the tissue level, for example, characteristic histopathological features defining the pathophysiology of ascending thoracic aortic aneurysms include degeneration of the elastin matrix, noninflammatory loss of SMCs, and biomechanical weakening of the aortic wall (Nataatmadja *et al.*, 2003). In this regard, our previous work revealed distinctions between the aneurysmal patient cohorts and nonaneurysmal, healthy aortic specimens at the cell, ECM, and tissue levels. Specifically, aneurysmal aortic specimens exhibited higher tensile strength, lower delamination strength, and anisotropic collagen and elastin fiber microarchitecture, and SMCs were more susceptible to oxidative stress than SMCs from degenerative aneurysm specimens and nonaneurysmal aortas (Phillippi *et al.*, 2009, 2010, 2014; Pichamuthu *et al.*, 2013; Tsamis *et al.*, 2014).

At the single-cell level, SMCs aid in supporting the surrounding ECM by generating contractile forces, or I-O forces, and resisting

This article was published online ahead of print in MBoC in Press (http://www.molbiolcell.org/cgi/doi/10.1091/mbc.E17-01-0053) on April 27, 2017.

*Address correspondence to: Julie A. Phillippi (phillippija@upmc.edu), Amrinder Nain (nain@vt.edu).

Abbreviations used: ECM, extracellular matrix; I-O, inside out; NFM, nanonet force microscopy; O-I, outside in; ROS, reactive oxygen species; SMC, smooth muscle cell; STEP, spinneret-based tunable engineered parameters.

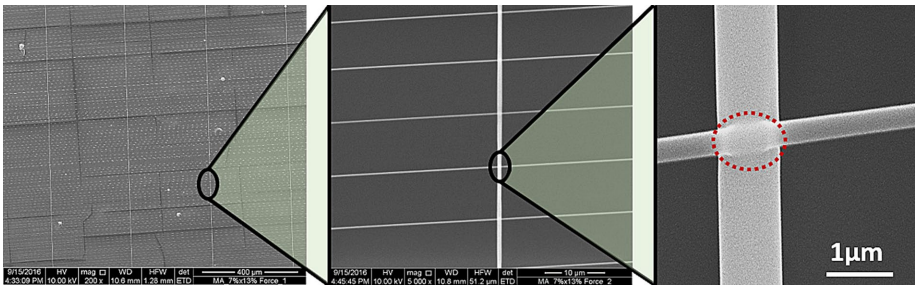

FIGURE 1: Fused-fiber nanonets. Scanning electron microscope images of nanonets spun over a hollowed-out scaffold such that large-diameter (~1000 nm), widely spaced fibers are orthogonal to and overlay small-diameter (250 nm), closely spaced fibers. Both fiber layers are fused at the intersections as shown by the red dashed oval. In such a configuration, cells interact exclusively with suspended fibers.

blood pressure expansion forces, or O-I forces (Chiu and Chien, 2011; Pasta *et al.*, 2013; Pichamuthu *et al.*, 2013). Using our previously reported nonelectrospinning spinneret-based tunable engineered parameters (STEP) technique (Nain *et al.*, 2008, 2009; Nain and Wang, 2013; Wang and Nain, 2014), we recently developed nanonet force microscopy (NFM; Figure 1) to measure both I-O and O-I forces at single-cell resolution (Sharma *et al.*, 2014; Sheets *et al.*, 2016). In this work, we apply the NFM platform to measure and compare I-O and O-I forces of SMCs (Figure 2 and Supplemental Movies S1 and S2) from three healthy human patient samples to evaluate baseline cell health. Furthermore, because reactive oxygen species (ROS) have been implicated in aneurysmal disease (Phillippi *et al.*, 2009; Folkersen *et al.*, 2011; Branchetti *et al.*, 2013) and potentially affect a cell's ability to produce and withstand forces, we determined the influence of ROS exposure on the SMC adhesive forces, thus providing further insight into the relationship between SMCs and ECM and how disease mechanisms could be studied using this platform. Measurement of human patient single-cell forces attached to ECM-mimicking fibers provides new means to calibrate cell forces across multiple patients, thus allowing the framework to study disease states and response to drugs.

RESULTS

I-O forces during migration and contractile state of SMC adhesion strength

Fused-fiber nanonets were fabricated using the nonelectrospinning STEP technique. Owing to the absence of an electric source in the fiber-spinning process, STEP enables precise control of fiber diameter, spacing, and orientation (Nain and Wang, 2013; Wang and Nain, 2014). Using STEP, we developed nanonets at ~15- to 20-µm spacing, to which cells attached in parallel morphologies with focal adhesions clustered predominantly at the poles (Sheets *et al.*, 2013). Cells use their focal adhesions to exert force on their substrate to spread or migrate. To calculate the vertical forces exerted by cells on fibers, the adhesion cluster lengths are modeled as point loads (Sheets *et al*, 2016). We observed that cells stretched between parallel fibers migrated by forming protrusions synchronously or asynchronously in an oscillatory manner on either fiber (Figure 3 and Supplemental Movie S3). This behavior was maintained among all three patient samples, thus suggesting an overall conserved behavior in cell migration on fibers. Next, to determine the contractile state of the cell, we averaged the total vertical force over 1 h for each cell and then averaged the forces for at least 11 cells per patient sample group. The average forces of the SMCs were found to be similar: 12.4 ± 2.4, 14.5 ± 1.4, and 12.9 ± 0.8 nN ($p = 0.30$; Figure 3C). Thus the average I-O force (12.9 ± 1.0 nN) for the three cell populations established the baseline contractile force for SMCs.

O-I force provides SMC–fiber adhesion strength

Using the same parallel-cell morphology, we measured the vertical O-I force by uniformly stretching the cell using custom dual probes positioned on either side of the cell. The probes were moved at a constant stretch rate of 2 µm/s, thus creating an active and passive fiber system (Figure 2B and Supplemental Movie S2). To measure the cell–fiber adhesion strength, we stretched cells until they detached from either of the two fibers. By using the two-point load model for the deflection of the passive fiber, we were thus able to calculate the maximum adhesion (O-I) force at detachment. A representative force–time plot in O-I perturbation shows an increase in the force, whereas adhesion integrity is maintained, followed by a sharp decrease, indicating cell–fiber adhesion failure (Figure 4A). O-I forces were calculated for the three cell lines with sample sizes of ≥7 cells/population to evaluate consistency across patients and develop a baseline SMC–fiber adhesion strength metric (Figure 4B). The mean O-I forces of the three populations were not statistically different ($p = 0.32$). Therefore we combined the O-I forces from the three populations to find an average maximum SMC O-I force of 57.9 ± 2.5 nN. Although the O-I forces were similar, during the experiments, we visually observed variations in cell sizes and that larger cells tended to produce higher forces

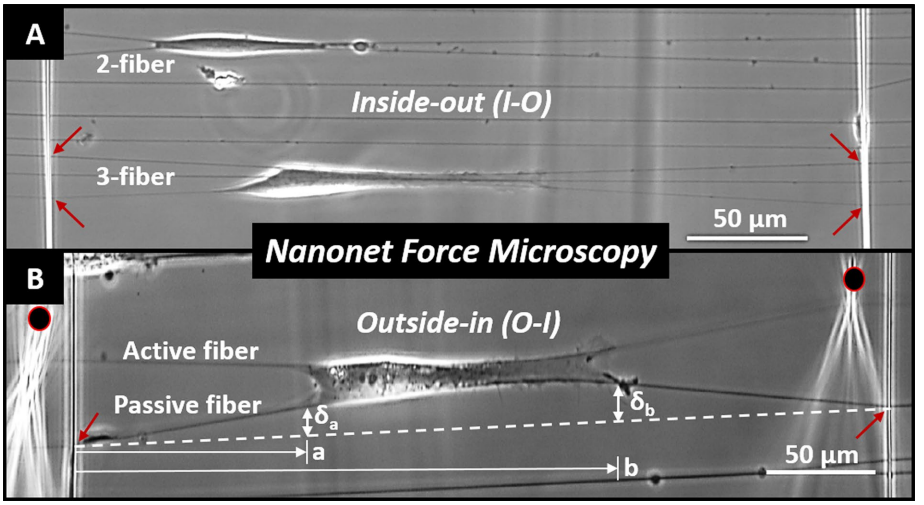

FIGURE 2: Optical image of SMCs attached to nanonets. (A) I-O force measurement in parallel shapes on two and three-fiber groups, and (B) O-I of single cell stretched by two probes on either side (black circles). Red arrows show representative fused-fiber intersections. Experimental measurements are shown only for the O-I case. The dashed white line represents the undeflected position of the fiber and δ_a, δ_b, *a*, and *b* the physical measurements made to estimate cell forces.

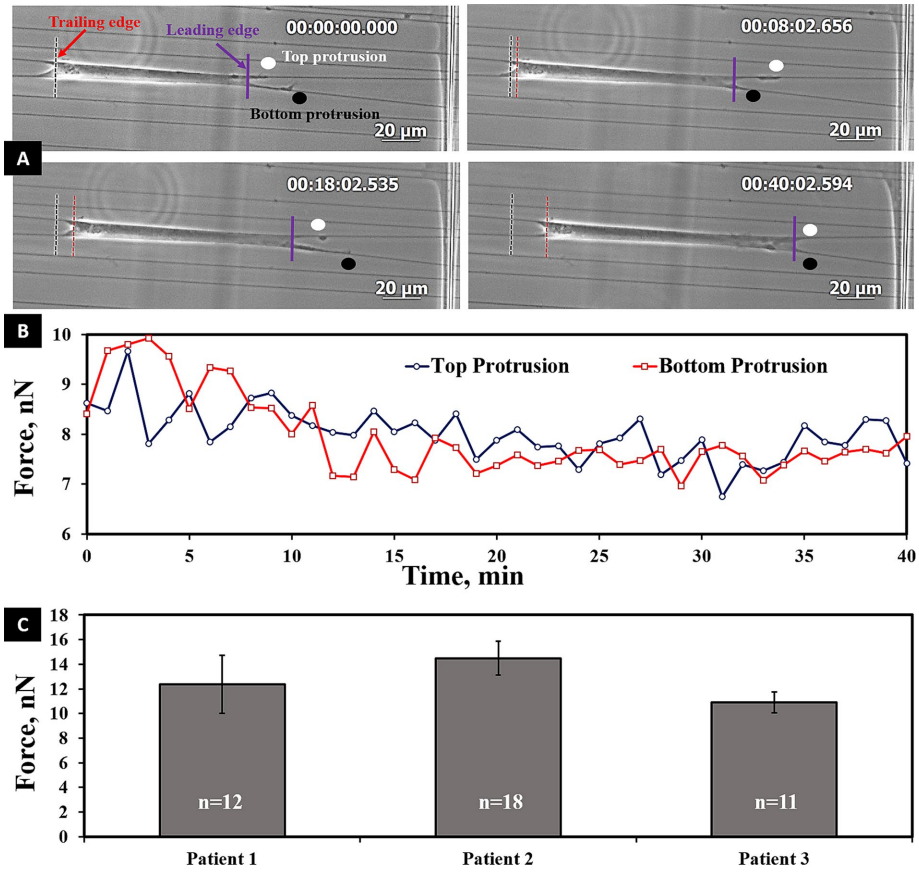

FIGURE 3: (A) Optical time-lapse images showing oscillatory pattern of protrusions on parallel fibers during cell migration. Time is shown in hours:minutes:seconds:thousandths. (B) Forces of top and bottom protrusions at the leading edge. (C) Average inside-out force values among three human patient samples. Statistically, these values were not significantly different ($p = 0.30$). Error bars represent standard error.

at failure. We performed linear least-squares regression analysis and found cell area and force at failure to be moderately correlated, with $R^2 = 0.494$ (Figure 4C) across all populations. This suggests that the size of individual cells may be related to the maximum O-I adhesion force. Combining the results, we find an approximately fivefold increase in the cell–fiber O-I compared with the passive contractile I-O forces ($p < 0.01$; Figure 4D).

Effects of oxidative stress and cyclic mechanical stress on adhesion force

To explore the influence of oxidative stress conditions in our force measurement platform, we exposed the SMCs to a pretreatment with hydrogen peroxide in the culture medium (oxidative stress conditions). The presence of hydrogen peroxide decreased both the single-cell I-O and O-I forces of human SMCs (Figure 5). The calculated I-O force in cells exposed to hydrogen peroxide was decreased by about one-half that of SMCs under normal culture conditions (5.6 ± 0.7 vs. 12.9 ± 1.0 nN; $p < 0.01$). We also observed a marked increase in the migration rates of cells under oxidative conditions (168.3 ± 18.1 vs. 70.7 ± 10.4 μm/h; $p = 0.011$; Figure 5A, inset, and Supplemental Movie S4). The effect of peroxide on O-I adhesion force was similar to that determined for I-O forces (30.2 ± 2.3 vs. 57.9 ± 2.5 nN; $p = 0.011$; Figure 5B).

Next we investigated the role of cyclic perturbation on passive contractile and cell–fiber adhesion strength modulation (Supplemental Movie S5). The cells were exposed to a cyclic, subfailure stretch (cell not detaching from fiber) for 1-, 5-, 10-, and 20-min intervals before a final O-I pull to failure (cell detaching from fiber). For all tested cyclic time intervals, we observed a decrease in both the passive contractile force and the O-I force (27.8 ± 3.9 vs. 57.9 ± 2.5 nN; $p < 0.01$; Figure 5, C–F). The reduction in I-O forces was consistent with our previous observation on reduction in forces with cyclic perturbations (Sheets *et al.*, 2016). I-O forces were reduced by similar amounts at 1- and 5-min cycles (6.8 ± 2.6 and 10.4 ± 2.8%; $p = 0.378$) but decreased significantly over long cycles (24.8 ± 4.2 and 64.8 ± 0.7% for 10 and 20 min, respectively; $p < 0.02$). However, of interest, the decrease in O-I forces occurred even at short intervals. Because cells tend to form focal adhesions at their poles on fibers, our data suggest that cyclic perturbations cause an active rearrangement of adhesions early, leading to reduced cell–fiber adhesion forces even at short cyclic times.

DISCUSSION

The platform presented here, to the best of our knowledge, is the first to measure human SMC single-cell–fiber forces in both passive and perturbed states. With our nanonet force platform, we established a baseline SMC contractile vertical force of 12.9 ± 1.0 nN across populations isolated from multiple patients. In the arterial system, particularly the aorta, tissue must also be able to withstand high O-I stretch forces that result from pulsatile contractions. By perturbing the cells, we established a reference vertical force of 57.9 ± 2.5 nN for healthy, nonaneurysmal SMCs. These passive and perturbed force calibrations could provide new insights in understanding, diagnosing, and developing preventive strategies for patients with cardiovascular disease.

SMCs bind to and interact with elastin and collagen fibers of the vascular ECM by exerting I-O contractile forces through actin–myosin contractions. The cells' ability to maintain these forces is necessary to preserve structural integrity and homeostasis of the tissue. For example, specimens of human aneurysm were shown to exhibit a loss of structural integrity, as demonstrated by decreased delamination strength of ascending aortic tissue, particularly for the aortopathy associated with bicuspid aortic valve (BAV; Nataatmadja *et al.*, 2003). Specimens from BAV-related aneurysm also exhibit a unique anisotropic ECM microarchitecture (Phillippi *et al.*, 2014), consistent with marked increases in unaxial tensile strength compared to normal, healthy specimens (Pichamuthu *et al.*, 2013). Thus there is a critical unmet need to develop enabling technologies that can recapitulate contextual in vivo environments while simultaneously affording access to cells for manipulation and study of putative disease pathways. Such new knowledge on cell–matrix interactions could have a major effect on public health, as 1–2% of the United States general population have BAV (Ward, 2000; Gleason, 2005), which carries a heightened risk of developing an aneurysm and is likely incited by different effector molecules than those causing degenerative aneurysm. In turn, presence of aneurysm places the

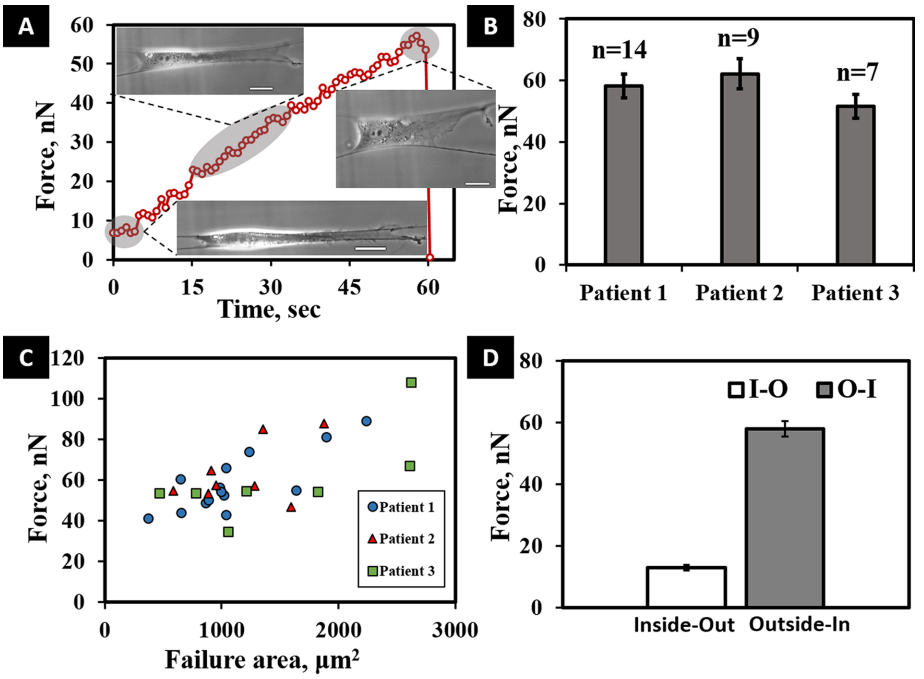

FIGURE 4: (A) Typical transient force response curve for a cell undergoing O-I perturbation, with a drop at 60 s indicating the maximum cell–fiber adhesion strength. Included in the figure are images of the same cell under different stretched conditions. Scale bars are 20 μm. (B) Average O-I forces for the three populations, with no significant variation. (C) Linear least-squares regression analysis shows failure forces and area at failure to be moderately correlated across all SMC populations undergoing O-I perturbation ($R^2 = 0.494$). (D) I-O and O-I vertical force comparison, with force values averaged across the cell populations, showing a fivefold difference in the I-O and O-I forces ($p < 0.01$). Error bars represent standard error.

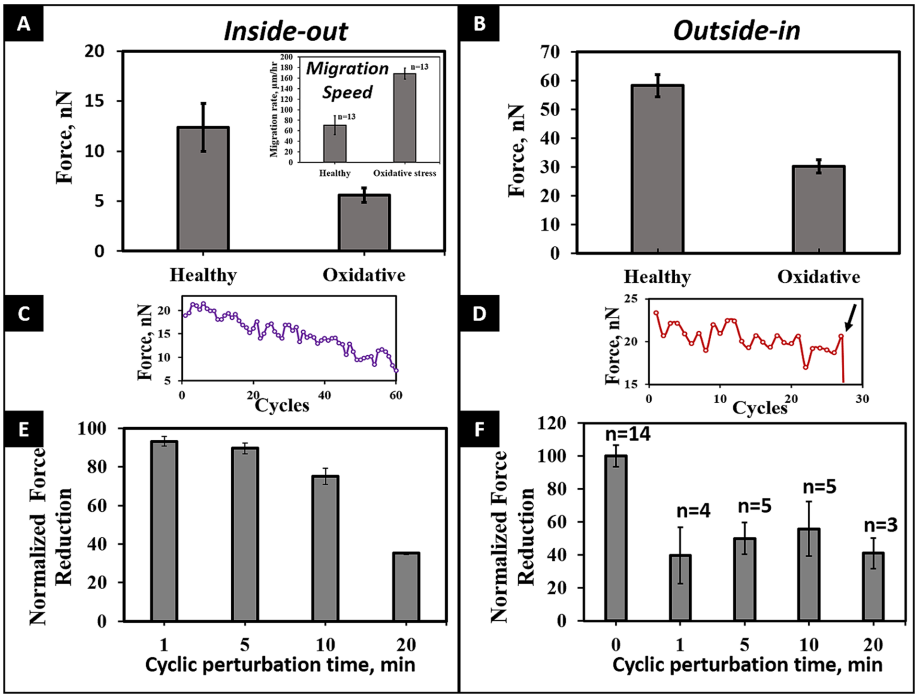

FIGURE 5: (A, B) Effect of oxidative stress on force modulation of SMCs for both I-O and O-I modes ($p < 0.01$ for both cases). Inset in A shows the higher migration rate of cells under oxidative conditions ($p < 0.01$). (C, D) Representative transient profiles of cyclic perturbation, showing decrease in force with increasing number of cycles and the detachment of the cell from the fiber in the O-I mode (arrow). (E) I-O forces decrease with increasing number of cycles. (F) O-I forces decrease with cyclic perturbation.

patient at risk for aortic catastrophe in the form of dissection and rupture, requiring immediate surgical intervention.

In pathological conditions, SMCs can be exposed to environmental stress (e.g., oxidative stress, reactive oxygen species [ROS], etc.); thus it is important to understand how I-O and O-I forces change in response under such conditions. In addition to the intracellular response, in this study we showed that exposure to oxidative stress reduces both I-O and O-I forces by about half that of cells under normal culture conditions. When we exposed the nonaneurysmal SMCs to cyclic loading, we observed that transient cell forces (both I-O and O-I) decreased over longer time intervals as cell stretch increased. Of interest, we found that cyclic loads and oxidative stress reduced the O-I forces to a similar degree. These findings in primary SMC and the enabling techniques support and enable our ongoing investigations related to SMC force mechanisms in the setting of BAV-associated aortopathy.

Oxidative stress has been of increasing interest in cardiovascular disease, with ROS linked to hypertension, atherosclerosis, and atrial fibrillation (Sahoo *et al.*, 2016). Our prior observations of human aortic specimens noted that medial SMCs isolated from specimens of BAV-associated aneurysm exhibited more oxidative stress–induced cell death than with normal aortic specimens and specimens of degenerative aneurysms (Phillippi *et al.*, 2009, 2010). Furthermore, primary SMCs isolated from BAV patients also exhibited down-regulation of the antioxidant metallothionein compared with normal aortic SMCs, implicating a role for oxidative stress response in BAV-associated aneurysmal disease. In addition, Branchetti *et al.* (2013) found that increased wall stress results in ROS accumulation, causing vascular smooth muscle cells to change toward a synthetic phenotype. The force measurement method described here for primary human SMCs will help us to further understand how SMC vulnerability to ROS in BAV-associated aortopathy influences the cell–matrix biomechanics that contribute to biomechanical integrity of the aortic wall. In addition, our nanonet approach to measuring SMC force generation will allow for testing the effect of modulating various cellular and matrix-related mechanisms toward our long-term goal of preventing or abating aneurysmal formation.

In conclusion, our studies emphasize that a combinatorial strategy of measuring both I-O and O-I forces should be implemented to develop a comprehensive understanding of the role of forces in cardiovascular disease.

With our contextually relevant nanonet force platform, we demonstrated that oxidative stress conditions result in perturbed adhesion forces in healthy, nonaneurysmal SMCs in complex in vitro structures that mimic the ECM milieu. The capability to alter the in vitro fibrous dimensions and measure corresponding force generation in human SMCs will be invaluable in understanding aortic wall integrity via cell–matrix adhesion. To our knowledge, this approach has never been applied to understand mechanisms of aortic aneurysmal disease. In the future, we plan to incorporate this platform to expand our studies of cell–cell and cell–matrix interactions in aortic disease pathologies at the cell–cell junctions and focal adhesion level, respectively, to aid in the development of therapeutic strategies to prevent progression of aneurysm and rupture of aorta.

MATERIALS AND METHODS

Nonelectrospinning STEP fused-fiber nanonets

The previously reported nonelectrospinning STEP technique was used to fabricate suspended criss-cross polystyrene nanonet scaffolds with fused-fiber interactions (Figure 1). Previous work from our group demonstrated that cells on suspended nanofibers tend to spread between two parallel fibers if the gap between them is <20 µm (Meehan and Nain, 2014). To increase the occurrence of this cell shape, the nanonets were configured such that strut-like, ~1000-nm-diameter fibers spaced ~300 µm apart were spun orthogonal to and on top of smaller, ~250-nm-diameter fibers with tighter spacing (15–20 µm apart).

Aortic tissue collection and SMC culture

Human ascending aortic specimens were collected from patients presenting for surgery to the Division of Cardiac Surgery, University of Pittsburgh Medical Center, for heart transplantation and were collected under Institutional Review Board approval and with informed patient consent or from organ donors via the Center for Organ Recovery and Education. Aortic specimens were collected from one male and two female patients ranging in age from 41 to 62 yr. Primary medial SMCs were isolated as previously described (Phillippi *et al.*, 2009). Three nonaneurysmal, cryopreserved SMC cell populations were reestablished in culture at passages 3–6 in 25-cm^2 flasks. The STEP scaffolds were fixated to the culture well of a glass-bottom six-well plate and glass-bottom dishes using sterile vacuum grease for I-O and O-I experiments, respectively. The fibers were sterilized by adding 1 ml of 70% ethanol for 10 min, followed by washing with phosphate-buffered saline. The fibers were then coated in 4 µg/ml fibronectin (Invitrogen, Carlsbad, CA) for 1–2 h to assist with cellular attachment onto the fibers (Sheets *et al.*, 2013). At 80% confluence, the cells were trypsinized and diluted in SMC medium (311K-500; Cell Applications) to a concentration of 30×10^4 cells/ml and then seeded on the scaffolds by placing 35 µl of droplets on top of the fiber grids. The cells were allowed to attach to fibers in an incubator at 37°C and 5% CO_2 for 4–6 h. Afterward, 2 ml of SMC medium was added to immerse the scaffold. For inducing oxidative stress, the cells were exposed to 125 µM hydrogen peroxide (Sigma-Aldrich), freshly diluted SMC medium for 30 min (Lennon *et al.*, 1991).

Imaging

For I-O and O-I measurements, after the cells were allowed to attach to the STEP fibers and 2 ml of SMC media had been added to the six-well plate, the plate was placed into an incubating microscope with a digital three-axis stage (AxioObserver Z1; Carl Zeiss, Germany). Cells were visualized using 20× magnification with an AxioCam MRm camera (Carl Zeiss). In I-O experiments, time lapse was performed with images captured at 1-min intervals, and care was taken to image cells in the parallel shape and avoid imaging cells in contact with other cells.

O-I forces were measured by placing glass micropipette probes mounted on a MP-285 motorized manipulator (Sutter) on either side of a parallel cell. To capture O-I force measurements, time-lapse images were taken every 600 ms. As with I-O forces, images were taken under 20× magnification. In oxidative stress condition experiments, cells were imaged for 15–20 min before adding the H_2O_2 medium to visualize transient force modulation. Force data were analyzed using a custom MATLAB code and the software ImageJ (National Institutes of Health, Bethesda, MD).

Force measurement

As cells attach and spread between parallel nanonet segments, the individual fibers deflect (Figure 2 and Supplemental Movie S1). In this configuration, cells form cell–fiber adhesion clusters on the periphery on each fiber (Meehan and Nain, 2014). Owing to these clusters, we assume that a cell applies two point loads on the fiber—one on each end of the cell–fiber interface (where the focal adhesions cluster)—which both contribute to overall fiber deflection (Sheets *et al.*, 2016). Thus the experimentally measured deflections, δ_a and δ_b (Figure 2B), can be related to their associated vertical loads, P_a and P_b (Sheets *et al.*, 2016):

$$\delta_a = \left(-\frac{P_a \sinh\left[\lambda(L-a)\right]}{S\lambda \sinh\left[\lambda L\right]} \sinh\left[\lambda a\right] + \frac{P_a (L-a)}{SL} a \right) - \frac{P_b \sinh\left[\lambda(L-b)\right]}{S\lambda \sinh\left[\lambda L\right]} \sinh\left[\lambda a\right] + \frac{P_b (L-b)}{SL} a$$

$$\delta_b = -\frac{P_a \sinh\left[\lambda a\right]}{S\lambda \sinh\left[\lambda L\right]} \sinh\left[\lambda(L-b)\right] + \frac{P_a (L-b)}{SL} a + \left(-\frac{P_b \sinh\left[\lambda(L-b)\right]}{S\lambda \sinh\left[\lambda L\right]} \sinh\left[\lambda b\right] + \frac{P_b (L-b)}{SL} b \right)$$

with the dependent variables defined in Table 1.

As cells migrate, they apply contractile forces on outer fibers, causing them to deflect (Figure 2A), from which I-O forces can be calculated. In the present study, we considered only cells attached to a two-fiber system. To develop the contractile force of the cell at any instant, we summed the individual fiber forces. To compare forces across different cells within and across SMC populations, we collected the I-O contractile forces and averaged them over 1 h of imaging. We compared these forces for three different human patients with a sample size of ≥11 cells/population.

O-I force is measured from cells in the same parallel morphology by uniformly pulling one of the fibers with a force probe until cell detachment, thus creating an active and passive fiber system (Figure 2B and Supplemental Movie S2). The deflection of the passive fiber is used to calculate force, and the point of cellular detachment from the passive fiber is considered the maximum O-I adhesion force of the cell to the fiber. The probes were fixed with their tips ~200 µm apart to account for larger cell widths and at a 45° angle to prevent the fiber slipping vertically during pulling. Using the manipulator, we positioned the probes parallel to and evenly spaced about the cell, providing uniform stretch to the cell in single and cyclic force perturbation modes. For cyclic mode, cells were cyclically stretched by programming 1-, 5-, 10-, and 20-min intervals at a strain rate of 2 µm/s before being pulled to adhesion failure. The cells were

Variable	Significance	Value
L	Segmental length of the fiber (distance between adjacent fixed ends)	~300 (μm)
a	Location of point load nearest to fiber-fiber intersection	$0 < a < L$ (μm)
b	Location of other point load	$0 < a < b < L$ (μm)
δ_a	Fiber deflection at a	Variable (μm)
δ_b	Fiber deflection at b	Variable (μm)
λ	Shape-dependent mechanics parameter	$\sqrt{S/EI}$ (m^{-1})
S	Uniform pretensional load	$S = \pi(d^2/4)T$ (μN)
T	Uniform pretensional stress, calculated from AFM residual stress measurements	4.1 MPa (Wang, 2015)
d	Fiber diameter	~250 nm
E	Elastic modulus of the polymer (polystyrene)	$E = 0.97$ (GPa) (Wang, 2015)
I	Area moment of inertia	$I = \frac{\pi d^4}{64}$ (m^4)

TABLE 1: STEP Nanonet force microscopy model parameters.

stretched to induce an initial 20-nN force, resulting in a frequency of 3 cycles/min.

Statistical analysis

I-O and O-I forces of the three populations were tested for statistical significance with one-way analysis of variance tests for difference of means to $p \leq 0.05$ (unless otherwise noted). The same test and p value were used to evaluate the effects of oxidative stress and cyclic loading to unstressed and nonloaded populations. Linear least-squares regression was also used to evaluate trends in cell area versus O-I force. Error bars represent standard error unless otherwise noted.

ACKNOWLEDGMENTS

T.G. and J.P. gratefully acknowledge Kristin Konopka and Julie Schreiber for assistance with IRB protocols and informed patient consent, Jennifer Hill and Tara Richards for smooth muscle cell isolation, and the Center for Organ Recovery and Education for assistance in obtaining donor tissues. T.G.G. and J.P. acknowledge support by the National Heart, Lung and Blood Institute of the National Institutes of Health under Award HL 109132 (T.G.G.) and the Department of Cardiothoracic Surgery at the University of Pittsburgh. A.S.N. acknowledges support by National Science Foundation Grants CMMI-1437101 and 1462916 and the Institute for Critical Technology and Applied Sciences at Virginia Tech.

REFERENCES

Branchetti E, Poggio P, Sainger R, Shang E, Grau JB, Jackson BM, Lai EK, Parmacek MS, Gorman RC, Gorman JH, *et al.* (2013). Oxidative stress modulates vascular smooth muscle cell phenotype via CTGF in thoracic aortic aneurysm. Cardiovasc Res 100, 316–324.

Chiu J-J, Chien S (2011). Effects of disturbed flow on vascular endothelium: pathophysiological basis and clinical perspectives. Physiol Rev 91, 327–387.

Folkersen L, Wågsäter D, Paloschi V, Jackson V, Petrini J, Kurtovic S, Maleki S, Eriksson MJ, Caidahl K, Hamsten A, *et al.* (2011). Unraveling divergent gene expression profiles in bicuspid and tricuspid aortic valve patients with thoracic aortic dilatation: the ASAP study. Mol Med 17, 1365–1373.

Gleason TG (2005). Heritable disorders predisposing to aortic dissection. Semin Thorac Cardiovasc Surg 17, 274–281.

Gunst SJ, Zhang W (2008). Actin cytoskeletal dynamics in smooth muscle: a new paradigm for the regulation of smooth muscle contraction. Am J Physiol Cell Physiol 295, C576–C587.

Lennon SV, Martin SJ, Cotter TG (1991). Dose-dependent induction of apoptosis in human tumour cell lines by widely diverging stimuli. Cell Prolif 24, 203–214.

Meehan S, Nain AS (2014). Role of suspended fiber structural stiffness and curvature on single-cell migration, nucleus shape, and focal-adhesion-cluster length. Biophys J 107, 2604–2611.

Moiseeva EP (2001). Adhesion receptors of vascular smooth muscle cells and their functions. Cardiovasc Res 52, 372–386.

Nain AS, Sitti M, Jacobson A, Kowalewski T, Amon C (2009). Dry spinning based spinneret based tunable engineered parameters (STEP) technique for controlled and aligned deposition of polymeric nanofibers. Macromol Rapid Commun 30, 1406–1412.

Nain AS, Phillippi JA, Sitti M, Mackrell J, Campbell PG, Amon C, Nain Phillippi JA, Sitti M, MacKrell K, Campbell PG, Amon CAS (2008). Control of cell behavior by aligned micro/nanofibrous biomaterial scaffolds fabricated by spinneret-based tunable engineered parameters (STEP) technique. Small 4, 1153–1159.

Nain AS, Wang J (2013). Polymeric nanofibers: isodiametric design space and methodology for depositing aligned nanofiber arrays in single and multiple layers. Polym J 45, 695–700.

Nataatmadja M, West M, West J, Summers K, Walker P, Nagata M, Watanabe T (2003). Abnormal extracellular matrix protein transport associated with increased apoptosis of vascular smooth muscle cells in marfan syndrome and bicuspid aortic valve thoracic aortic aneurysm. Circulation 108 (Suppl II), 329–334.

Pasta S, Rinaudo A, Luca A, Pilato M, Scardulla C, Gleason TG, Vorp DA (2013). Difference in hemodynamic and wall stress of ascending thoracic aortic aneurysms with bicuspid and tricuspid aortic valve. J Biomech 46, 1729–1738.

Phillippi JA, Eskay MA, Kubala AA, Pitt BR, Gleason TG (2010). Altered oxidative stress responses and increased type I collagen expression in bicuspid aortic valve patients. Ann Thorac Surg 90, 1893–1898.

Phillippi JA, Green BR, Eskay MA, Kotlarczyk MP, Hill MR, Robertson AM, Watkins SC, Vorp DA, Gleason TG (2014). Mechanism of aortic medial matrix remodeling is distinct in patients with bicuspid aortic valve. J Thorac Cardiovasc Surg 147, 1056–1064.

Phillippi JA, Klyachko EA, Kenny JP, Eskay MA, Gorman RC, Gleason TG (2009). Basal and oxidative stress-induced expression of metallothionein

is decreased in ascending aortic aneurysms of bicuspid aortic valve patients. Circulation 119, 2498–2506.
Pichamuthu JE, Phillippi JA, Cleary DA, Chew DW, Hempel J, Vorp DA, Gleason TG (2013). Differential tensile strength and collagen composition in ascending aortic aneurysms by aortic valve phenotype. Ann Thorac Surg 96, 2147–2154.
Sahoo S, Meijles DN, Pagano PJ (2016). NADPH oxidases: key modulators in aging and age-related cardiovascular diseases? Clin Sci 130, 317–335.
Sharma P, Kim A, Gill A, Wang J, Sheets K, Behkam B, Nain AS (2014). Aligned and suspended fiber force probes for drug testing at single cell resolution. Biofabrication 6, 45006.
Sheets K, Wang J, Zhao W, Kapania R, Nain AS (2016). Nanonet force microscopy for measuring cell forces. Biophys J 111, 197–207.
Sheets K, Wunsch S, Ng C, Nain AS (2013). Shape-dependent cell migration and focal adhesion organization on suspended and aligned nanofiber scaffolds. Acta Biomater 9, 7169–7177.
Tsamis A, Pal S, Phillippi JA, Gleason TG (2014). Effect of aneurysm on biomechanical properties of "radially-oriented" collagen fi bers in human ascending thoracic aortic media. J Biomech 47, 3820–3824.
Wang J (2015). Hierarchical Advanced Materials of Nanofibers in Single and Multiple Layers. PhD Thesis. Blacksburg: Virginia Tech.
Wang J, Nain AS (2014). Suspended micro/nanofiber hierarchical biological scaffolds fabricated using non-electrospinning STEP technique. Langmuir 30, 13641–13649.
Ward C (2000). Clinical significance of the bicuspid aortic valve. Heart 83, 81–85.